

Modeling of defect modes in photonic crystals using the fictitious source superposition methodS. Wilcox,¹ L. C. Botten,² R. C. McPhedran,¹ C. G. Poulton,³ and C. Martijn de Sterke¹¹*Centre for Ultrahigh-bandwidth Devices for Optical Systems (CUDOS) and School of Physics, University of Sydney, Sydney, New South Wales 2006, Australia*²*Centre for Ultrahigh-bandwidth Devices for Optical Systems (CUDOS) and Department of Mathematical Sciences, University of Technology, Sydney, New South Wales 2007, Australia*³*High Frequency and Quantum Electronics Laboratory, University of Karlsruhe, 78128 Karlsruhe, Germany*

(Received 13 December 2004; published 12 May 2005)

We present an exact theory for modeling defect modes in two-dimensional photonic crystals having an infinite cladding. The method is based on three key concepts, namely, the use of fictitious sources to modify response fields that allow defects to be introduced, the representation of the defect mode field as a superposition of solutions of quasiperiodic field problems, and the simplification of the two-dimensional superposition to a more efficient, one-dimensional average using Bloch mode methods. We demonstrate the accuracy and efficiency of the method, comparing results obtained using alternative techniques, and then concentrate on its strengths, particularly in handling difficult problems, such as where a mode is highly extended near cutoff, that cannot be dealt with in other ways.

DOI: 10.1103/PhysRevE.71.056606

PACS number(s): 42.70.Qs, 42.79.Dj

I. INTRODUCTION

Photonic crystals [1] (PCs) and photonic crystal fibers [2] (PCFs) are structures in which the refractive index depends periodically on position. Many of the exciting light propagation properties of these structures arise from the existence of photonic band gaps, frequency intervals in which running wave solutions are not allowed. In this paper, we concern ourselves with structures with a two-dimensional plane of periodicity. In PCs, the light propagates in this plane, and the refractive index in the direction orthogonal to this plane is designed for light confinement in that direction. However, for simplicity these structures are often modeled as being uniform in this direction, so that only a two-dimensional calculation is required. In PCFs the refractive index in the direction orthogonal to the plane of periodicity genuinely is uniform, but in contrast to two-dimensional PCs, the light propagation is not confined to this plane.

Many applications of PCs and PCFs rely on the introduction of defects in an otherwise periodic structure: in PCs, line defects lead to waveguides [3], whereas localized defects give rise to resonators [4,5], while in PCFs, a localized defect forms the core of the fiber [6]. These applications require a photonic band gap to confine the light to these defects. Until now, almost all the modeling of PCs or PCFs with defects has used one of two general methods. The first of these are supercell methods, by which the geometry is repeated periodically [7–9]. This turns a nonperiodic structure into one with periodicity, so that methods that have been developed for periodic structures, relying principally on Bloch's theorem, can be brought to bear. The use of such a procedure is justified when the size of the supercell exceeds the size of any of the features that are to be modeled since, otherwise, artificial overlaps are introduced. The second class of methods to deal with periodic structures with defects model these structures as being of finite extent [10–12] (often with the use of appropriate absorbing boundary conditions to make finite the solution region). Of course, this is

well justified since real systems are finite. However, these methods tend not to be very efficient since an overarching mathematical framework, such as Bloch's theorem, is missing. Accordingly, the physical size of the systems that can be modeled is limited.

Photonic crystal waveguides may be studied also using methods that fit into neither of the two categories mentioned above. These methods [13] make use of the reflection scattering matrix of semi-infinite photonic crystals [14]. This matrix \mathbf{R}_∞ describes the response of a semi-infinite photonic crystal to an incident plane wave of given frequency, polarization, and direction. The response consists of a number of reflected plane waves at angles given by the grating equation, and an infinite number of evanescent orders. The columns of \mathbf{R}_∞ contain the amplitudes of the reflected waves generated by the respective incoming plane wave orders of unit amplitude. Thus, with this tool, a straight photonic crystal waveguide can be modeled as a conventional waveguide: it consists of a uniform medium, sandwiched between two semi-infinite media, the response of which is completely determined by \mathbf{R}_∞ , and by the separation of the semi-infinite media. In such calculations the modes are found by applying a phase or resonance condition. Calculations of this type, which model a genuinely infinite system, have advantages over conventional methods involving a supercell: they are not only more elegant, but they are also efficient since the calculation of \mathbf{R}_∞ involves the Bloch functions of the infinite system. They are also particularly well suited to calculations when the modal fields have a large extent (such as occurs close to modal cutoff), since the modeling of these fields would require a very large supercell.

By construction, the method described in the previous paragraph applies only to line defects, but not to defects that are localized. In this paper, however, we describe a method for calculating the modes of localized defects in otherwise infinite structures, both in PCs and in PCFs. This *fictitious source superposition (FSS) method* shares the advantages listed above: it is theoretically elegant, analytically tractable,

and can calculate modes of large spatial extent efficiently. The latter is important in the study of PCFs, where the properties of the fundamental mode at long wavelengths are not well understood. The long-wavelength behavior can only be resolved by the type of method described here.

There are three key ideas involved in the development and implementation of the FSS method. The *first* is the application of fictitious sources which, when introduced into the interior of any scatterer, allow the field exterior to the scatterer to be tailored. Here, we exploit a fictitious source, either to make the scatterer vanish, in that the exterior field is identical to that if the scatterer was not present, or to modify its electromagnetic response so that it mimics the behavior of a scatterer with different size or optical properties. The fictitious source required to modify the response of an individual scatterer depends on the field incident upon that scatterer. While the calculations are straightforward for a problem involving only a single scatterer, the interrelationships between the fields in an infinite array of scatterers are complex and make it difficult to solve the field problem directly.

This brings us to the *second* key idea, the construction of the defect mode from a superposition of quasiperiodic field solutions for the perfectly periodic structure. For each of the constituent problems, we embed a source \mathbf{Q}_p in each scatterer and phase these quasiperiodically such that $\mathbf{Q}_p = \mathbf{Q} \exp(i\mathbf{k}_0 \cdot \mathbf{R}_p)$ where \mathbf{R}_p is the lattice position of scatterer p . The defect mode is then formed by a superposition of the solutions of the periodic structure by integrating with respect to the Bloch vector \mathbf{k}_0 over the first Brillouin zone. The superposed solution thus satisfies the relevant wave equation, the boundary conditions, and is associated with a fictitious source distribution in which scatterer p contains the source $\mathbf{Q} \int_{\text{BZ}} \exp(i\mathbf{k}_0 \cdot \mathbf{R}_p) d\mathbf{k}_0$. This is the key step, with the Brillouin zone integration entirely eliminating the fictitious sources [15] in all but the primary scatterer ($\mathbf{R}_p=0$). The remaining source, in the primary scatterer, is thus available to modify the response field and, in doing so, to formulate the defect mode.

For the two-dimensional structures that we are considering, the Brillouin zone integration requires a time consuming two-dimensional calculation. The efficiency of the calculation can be increased dramatically by reformulating the problem so that only a one-dimensional integration is required. This reformulation of the problem is the *third* key idea, and models the structure as a single diffraction grating with embedded quasiperiodically phased fictitious sources, that is sandwiched between two semi-infinite photonic crystals that are modeled by \mathbf{R}_∞ [14]. These are crucial to this approach in that they encapsulate the second dimension of the Brillouin zone in their mode structure, eliminating one integration direction, and thus reducing the solution of the problem to require only a one-dimensional Brillouin zone integration.

In Sec. II, we formulate the method for two-dimensional cylinder arrays for both elementary polarizations, and then outline the generalization to handle out-of-plane configurations required for PCFs. We then discuss the numerical implementation in Sec. III, and verify the method in Sec. IV. In Sec. V, we conclude by considering the challenging case of modeling defect modes that are highly extended.

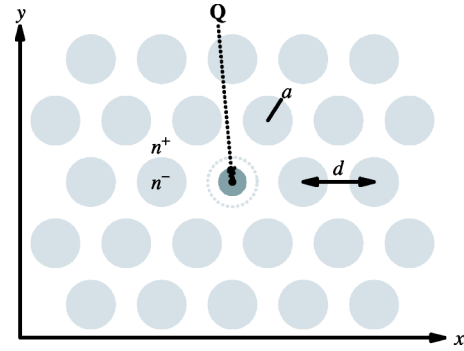


FIG. 1. Schematic of the geometry with cylinders of radius a and refractive index n^- , in a background index n^+ . A defect is formed by either removing the central cylinder or changing its radius or refractive index; mathematically, this defect is modeled by considering a perfectly periodic structure and inserting a source into the central cylinder (dotted).

II. THEORY

We begin with the geometry to be modeled (Sec. II A), and introduce the multipole method on which the FSS method is based. Section II B presents the plane wave scattering matrices [16,17] which describe a grating with embedded sources, while Sec. II C summarizes the calculation of the matrix \mathbf{R}_∞ which describes the reflection of a semi-infinite PC. Finally, in Sec. II D we combine the properties of these two structures to model a periodic structure with sources placed along the central row to calculate the modes for waveguides and point defects.

A. Preliminaries

Our aim is to model the structure shown in Fig. 1: dielectric cylindrical inclusions of radius a and refractive index n^- in a dielectric background material of index n^+ , with axes aligned with the \hat{z} axis. These are placed on some regular lattice with lattice vectors \mathbf{e}_1 and \mathbf{e}_2 and the central cylinder is either removed or altered to form a defect. Since initially we deal with two-dimensional problems, in which the fields are independent of z , we can assume that either the electric or magnetic field lies along the z axis. These polarizations are denoted \mathbf{E}_\parallel and \mathbf{H}_\parallel , respectively. The z component of the relevant field is denoted V ; the other field has no z component.

The theory relies on the multipole method [10,16], which was developed to model dielectric structures with cylindrical inclusions. Central to the multipole method are the local field expansions or *multipole expansions* around each inclusion. Assume cylinder j is centered at \mathbf{c}^j . Because V satisfies a Helmholtz equation inside and outside the cylinder, we can write, in cylindrical coordinates, $\mathbf{r}=(r, \theta)$,

$$V(\mathbf{c}^j + \mathbf{r}) = \sum_{l=-\infty}^{\infty} [A_l^j J_l(k^+ r) + B_l^j H_l^{(1)}(k^+ r)] e^{il\theta},$$

$$V(\mathbf{c}^j + \mathbf{r}) = \sum_{l=-\infty}^{\infty} [C_l^j J_l(k^- r) + Q_l^j H_l^{(1)}(k^- r)] e^{il\theta}, \quad (1)$$

for $r \geq a$ and $r \leq a$, respectively. Here $k^\pm = kn^\pm$ denote the magnitudes of the wave number inside and outside the cyl-

inder. Also J_l and $H_l^{(1)}$ denote the Bessel function of the first kind and the Hankel function of the first kind, respectively. For convenience the latter is denoted by H_l from this point. Also, in what follows, we formulate the problem in a vector-matrix notation, denoting such quantities by boldface symbols, e.g., $\mathbf{A}^j = [A_l^j]$ represents a vector of coefficients. Physically, the coefficients \mathbf{A}^j represent the standing wave field incident on the cylinder, \mathbf{B}^j is the field outgoing from the cylinder, \mathbf{C}^j is that inside the cylinder, incoming from the cylinder's boundary, and \mathbf{Q}^j represents a fictitious source inside the cylinder. The last is used to tailor the fields outside the cylinder, so that it disappears or mimics a different cylinder. To achieve this we consider the relationships between the coefficients inside and outside the cylinder, that result from the continuity conditions of the fields at the cylinder's boundary. They can be written

$$\begin{aligned}
 \mathbf{B}^j &= \hat{\mathbf{R}}\mathbf{A}^j + \hat{\mathbf{T}}\mathbf{Q}^j, \\
 \mathbf{C}^j &= \hat{\mathbf{T}}'\mathbf{A}^j + \hat{\mathbf{R}}'\mathbf{Q}^j.
 \end{aligned} \quad (2)$$

These equations express the outgoing field \mathbf{B}^j as a reflection of the incoming field \mathbf{A}^j and a transmission of the internal source \mathbf{Q}^j , and similarly for \mathbf{C}^j ; that is, the matrices $\hat{\mathbf{R}}$, $\hat{\mathbf{T}}$, $\hat{\mathbf{R}}'$, and $\hat{\mathbf{T}}'$ are essentially Fresnel coefficients in the cylindrical harmonic basis. Because the local field expansion in cylindrical coordinates is well suited to the cylindrical shape of the inclusions, these matrices are diagonal. The second equation is used only for field reconstruction, and is not mentioned again. Explicit forms for the elements of these matrices are given in Refs. [10,18].

We now exploit Eqs. (2) to illustrate the first key idea, by removing a single cylinder. The condition on the external fields for the cylinder to disappear is $\mathbf{B}^j=0$, i.e., there is no outgoing field sourced by this cylinder. From Eq. (2), we deduce that the required source is

$$\mathbf{Q}^j = -\hat{\mathbf{T}}^{-1}\hat{\mathbf{R}}\mathbf{A}^j,$$

which depends on the incident field \mathbf{A}^j . As noted in the Introduction, the direct extension of this idea to modeling a defect mode in an infinite lattice is very difficult, if not possible, given the complex interactions between the scatterers. Instead, we develop the mode through a superposition of quasiperiodic fictitious sources (Sec. II D) as was outlined earlier.

B. The grating field problem

Recalling the third key idea discussed in Sec. I, we now model a cylinder grating, with cylinders placed along the x axis with period d (Fig. 2), and having embedded sources. From Bloch's theorem, the x periodicity of the grating allows us to apply the quasiperiodicity condition

$$V(\mathbf{r} + d\hat{\mathbf{x}}) = e^{i\alpha_0 d} V(\mathbf{r}),$$

where α_0 is the lateral component of the Bloch vector \mathbf{k}_0 . This quasiperiodicity implies that the multipole expansion coefficients (1) around the j th cylinder of the grating are given by

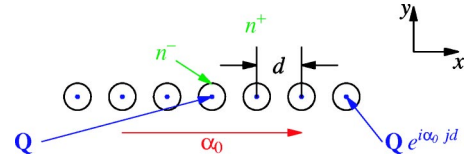


FIG. 2. A grating is formed by a row of cylinders, with their axes aligned along the z axis (out of the plane). Such gratings are stacked to model the desired structure in Fig. 1. Here the cylinders also contain sources as shown.

$$\begin{aligned}
 \mathbf{A}^j &= e^{i\alpha_0 j d} \mathbf{A}, & \mathbf{B}^j &= e^{i\alpha_0 j d} \mathbf{B}, \\
 \mathbf{C}^j &= e^{i\alpha_0 j d} \mathbf{C}, & \mathbf{Q}^j &= e^{i\alpha_0 j d} \mathbf{Q},
 \end{aligned}$$

where the omission of the index j refers to the central cylinder ($j=0$).

The form of the field expansion around the central cylinder is determined by a relation between the singular and nonsingular parts of the field, known as the Rayleigh identity. To derive this we apply Green's theorem in the unit cell, using the field V and the quasiperiodic Green's function, which satisfies

$$(\nabla^2 + k^2)G(\mathbf{r}) = \sum_{j=-\infty}^{\infty} \delta(\mathbf{r} - j d\hat{\mathbf{x}}) e^{i\alpha_0 j d}.$$

In cylindrical coordinates [$\mathbf{r}=(r, \theta)$] the quasiperiodic Green's function can be written

$$\begin{aligned}
 G(\mathbf{r}) &= -\frac{i}{4} \sum_{j=-\infty}^{\infty} e^{i\alpha_0 j d} H_0(k^+|\mathbf{r} - j d\hat{\mathbf{x}}|) \\
 &= -\frac{i}{4} H_0(k^+r) - \frac{i}{4} \sum_{l=-\infty}^{\infty} S_l J_l(k^+r) e^{il\theta}.
 \end{aligned} \quad (3)$$

A second form of the Green's function in Eq. (3), which applies when $r < d$, is obtained using Graf's addition theorem and introduces the *lattice sums* [14] defined by

$$S_l = \sum_{j=1}^{\infty} H_l(k^+ j d) [e^{i\alpha_0 j d} + (-1)^l e^{-i\alpha_0 j d}],$$

characterizing the contributions to each multipole order due to the phased array of multipole sources. It is this particular form of the Green's function (3) that ultimately yields the field (Rayleigh) identity, with the first term $H_0(k^+r)$ referring to an outgoing wave generated by the primary source ($j=0$), and the second term, comprising a sum of terms $J_l(k^+r)\exp(il\theta)$ weighted by the lattice sums, and representing an incident field that is generated by all other sources.

We now apply Green's theorem to derive the field expansion in the vicinity of the primary cylinder, denoting by C the boundary of central cylinder and by D the boundary of a unit cell of the grating, both traversed counterclockwise. Applying Green's theorem to $V(\mathbf{r}_1)$ and $G(\mathbf{r}-\mathbf{r}_1)$ in the region R between C and D gives

$$\begin{aligned}
V(\mathbf{r}) &= \oint_C \left[G(\mathbf{r}-\mathbf{r}_1) \frac{\partial V}{\partial \hat{\mathbf{n}}_1}(\mathbf{r}_1) - V(\mathbf{r}_1) \frac{\partial G}{\partial \hat{\mathbf{n}}_1}(\mathbf{r}-\mathbf{r}_1) \right] d\mathbf{r}_1 \\
&+ \oint_D \left[V(\mathbf{r}_1) \frac{\partial G}{\partial \hat{\mathbf{n}}_1}(\mathbf{r}-\mathbf{r}_1) - G(\mathbf{r}-\mathbf{r}_1) \frac{\partial V}{\partial \hat{\mathbf{n}}_1}(\mathbf{r}_1) \right] d\mathbf{r}_1 \\
&= I_C + I_D,
\end{aligned} \quad (4)$$

for any $\mathbf{r} \in R$. We obtain an expression for $G(\mathbf{r}-\mathbf{r}_1)$ from the form given in Eq. (3), together with a further application of Graf's addition theorem. Then, using the multipole expansion (1) around the central cylinder for V , we evaluate

$$I_C = \sum_{l=-\infty}^{\infty} B_l H_l(k^+ r) e^{il\theta} + \sum_{l=-\infty}^{\infty} J_l(k^+ r) e^{il\theta} \sum_{m=-\infty}^{\infty} S_{l-m} B_m, \quad (5)$$

for \mathbf{r} sufficiently close to the central cylinder.

To evaluate the integral over D , we decompose the field above and below the grating into plane waves of the correct quasiperiodicity. That is,

$$\begin{aligned}
V(\mathbf{r}) &= \sum_{p=-\infty}^{\infty} \chi_p^{-1/2} e^{i\alpha_p x} (f_{1p}^+ e^{i\chi_p y} + f_{1p}^- e^{-i\chi_p y}), \\
V(\mathbf{r}) &= \sum_{p=-\infty}^{\infty} \chi_p^{-1/2} e^{i\alpha_p x} (f_{2p}^+ e^{i\chi_p y} + f_{2p}^- e^{-i\chi_p y}),
\end{aligned}$$

for $y > a$ and $y < -a$, respectively, where

$$\alpha_p = \alpha_0 + \frac{2\pi}{d} p = k^+ \sin \theta_p,$$

$$\chi_p = \sqrt{(k^+)^2 - \alpha_p^2} = k^+ \cos \theta_p$$

denote the direction sines and cosines of the relevant diffraction orders. The plane wave coefficients f_1^- and f_2^+ represent the incoming plane waves above and below the grating respectively, while f_1^+ and f_2^- represent the outward-going plane waves. The factor $\chi_p^{-1/2}$ is a convenient normalization [16] which ensures that each propagating plane wave order carries unit energy flux.

The evaluation of I_D requires the plane wave form of the Green's function (3)

$$G(\mathbf{r}) = \frac{1}{2id} \sum_{q=-\infty}^{\infty} \frac{1}{\chi_q} e^{i(\alpha_q x + \chi_q |y|)}. \quad (6)$$

Using this, the left and right sides of the integral along D cancel due to quasiperiodicity and we obtain

$$I_D = \sum_{p=-\infty}^{\infty} \chi_p^{-1/2} e^{i\alpha_p x} (f_{1p}^- e^{i\chi_p y} + f_{2p}^+ e^{i\chi_p y}), \quad (7)$$

namely, the plane wave field incident upon the grating. To proceed further, we need to convert this form to the cylindrical harmonic (multipole) basis, deriving

$$I_D = \sum_{p=-\infty}^{\infty} \sum_{l=-\infty}^{\infty} (J_{0lp}^- f_{1p}^- + J_{0lp}^+ f_{2p}^+) J_l(k^+ r) e^{il\theta}, \quad (8)$$

where

$$J_{0lp}^+ = \chi_p^{-1/2} e^{il\theta_p}, \quad J_{0lp}^- = \chi_p^{-1/2} (-1)^l e^{-il\theta_p}.$$

Then, substituting Eqs. (5) and (8) into Eq. (4), we obtain the total field expansion

$$\begin{aligned}
V(\mathbf{r}) &= \sum_l B_l H_l(k^+ r) e^{il\theta} + \sum_l J_l(k^+ r) e^{il\theta} \sum_m S_{l-m} B_m \\
&+ \sum_p \sum_l (J_{0lp}^- f_{1p}^- + J_{0lp}^+ f_{2p}^+) J_l(k^+ r) e^{il\theta},
\end{aligned} \quad (9)$$

valid for \mathbf{r} sufficiently close to the central cylinder. The expansion in Eq. (9) comprises three terms, an outgoing field sourced at the primary cylinder, an incident field that is due to all other cylinders, and the incoming plane waves. Equating this with the local expansion (1) for the central cylinder ($j=0$) and comparing the coefficients of terms $e^{il\theta}$, we deduce the Rayleigh identity

$$A_l = \sum_{m=-\infty}^{\infty} S_{lm} B_m + \sum_{p=-\infty}^{\infty} (J_{0lp}^- f_{1p}^- + J_{0lp}^+ f_{2p}^+),$$

where $S_{lm} = S_{l-m}$. That is, in the vicinity of the central cylinder, the nonsingular part of the field (i.e., that part of the field that is not outgoing from that cylinder) is due to all other cylinders and incident plane waves. In matrix notation, this reduces to

$$\mathbf{A} = \mathbf{S}\mathbf{B} + \mathbf{J}_0^- \mathbf{f}_1^- + \mathbf{J}_0^+ \mathbf{f}_2^+. \quad (10)$$

As we have seen above, I_C represents the quasiperiodic field that is outgoing from the grating. We can derive an alternative form for this by using the plane wave form of the Green's function $G(\mathbf{r}-\mathbf{r}_1)$ from Eq. (6). Maintaining the field point (\mathbf{r}) dependence in Cartesian exponential form, and transforming the source point $[\mathbf{r}_1 = (r_1, \theta_1)]$ dependent exponential terms into cylindrical harmonics [i.e., $J_l(k^+ r_1) e^{il\theta_1}$], the integral I_C may then be evaluated to yield the outgoing plane waves in terms of the multipole coefficients \mathbf{B} . That is,

$$I_C = \frac{2}{d} \sum_{p=-\infty}^{\infty} \sum_{l=-\infty}^{\infty} \chi_p^{-1/2} e^{i(\alpha_p x \pm \chi_p y)} K_{0pl}^\pm B_l, \quad (11)$$

where the $+$ and $-$ signs correspond to $y > a$ and $y < -a$, respectively, and

$$K_{0pl}^+ = \frac{2}{d} \chi_p^{-1/2} e^{-il\theta_p}, \quad K_{0pl}^- = \frac{2}{d} \chi_p^{-1/2} (-1)^l e^{il\theta_p}.$$

Then, substituting Eqs. (7) and (11) into Eq. (4) gives

$$\begin{aligned}
V(\mathbf{r}) &= \sum_{p=-\infty}^{\infty} \chi_p^{-1/2} e^{i\alpha_p x} (f_{1p}^- e^{-i\chi_p y} + f_{2p}^+ e^{i\chi_p y}) \\
&+ \sum_{p=-\infty}^{\infty} \sum_{l=-\infty}^{\infty} \chi_p^{-1/2} K_{0pl}^\pm B_l e^{i(\alpha_p x \pm \chi_p y)}.
\end{aligned}$$

As in Eq. (9), we have expressed the field as a sum of contributions from fields incident on the grating, and fields outgoing from the cylinders. However, in this expression, we have converted the latter into plane waves using \mathbf{K}_0^\pm , rather than converting the former into cylindrical harmonic functions using \mathbf{J}_0^\pm . When this expansion is compared with the plane wave expansion above or below the grating, one of the terms in the first sum cancels. Equating coefficients of the plane wave orders then gives

$$f_{1p}^+ = f_{2p}^+ + \sum_{m=-\infty}^{\infty} K_{0pl}^+ B_l,$$

$$f_{2p}^- = f_{1p}^- + \sum_{m=-\infty}^{\infty} K_{0pl}^- B_l,$$

or, in matrix notation,

$$\begin{aligned} \mathbf{f}_1^+ &= \mathbf{f}_2^+ + \mathbf{K}_0^+ \mathbf{B}, \\ \mathbf{f}_2^- &= \mathbf{f}_1^- + \mathbf{K}_0^- \mathbf{B}, \end{aligned} \quad (12)$$

the first expressing that the upward field above the grating (\mathbf{f}_1^+) is due to the upward field from below (\mathbf{f}_2^+) and the upward field generated by the grating ($\mathbf{K}_0^+ \mathbf{B}$).

Expressions (10) and (12) relate the different field expansions outside the cylinders, and incorporate the geometrical arrangement of the cylinders. When this is combined with the multipole relations of Eq. (2), which incorporate the material properties (i.e., radius and optical constants) of the individual cylinders, we derive the reflection and transmission characteristics of the grating with embedded sources. By substituting Eq. (10) into Eq. (2) we derive an expression for the outgoing multipole field coefficients \mathbf{B} as a function of the ‘‘forcing terms,’’ namely, the fictitious sources \mathbf{Q} and the incident plane wave fields \mathbf{f}_1^+ and \mathbf{f}_2^+ . That is,

$$\mathbf{B} = \mathbf{G}(\hat{\mathbf{R}}\mathbf{J}_0^- \mathbf{f}_1^+ + \hat{\mathbf{R}}\mathbf{J}_0^+ \mathbf{f}_2^+ + \hat{\mathbf{T}}\mathbf{Q}), \quad (13)$$

where

$$\mathbf{G} = (\mathbf{1} - \hat{\mathbf{R}}\mathbf{S})^{-1},$$

and $\mathbf{1}$ denotes the identity matrix. Finally, by combining Eqs. (13) and (12), we deduce

$$\begin{aligned} \mathbf{f}_1^+ &= \mathbf{R}_0^+ \mathbf{f}_1^- + \mathbf{T}_0^+ \mathbf{f}_2^+ + \mathbf{Q}_0^+ \mathbf{Q}, \\ \mathbf{f}_2^- &= \mathbf{R}_0^- \mathbf{f}_2^+ + \mathbf{T}_0^- \mathbf{f}_1^- + \mathbf{Q}_0^- \mathbf{Q}, \end{aligned} \quad (14)$$

where

$$\begin{aligned} \mathbf{R}_0^+ &= \mathbf{K}_0^+ \hat{\mathbf{G}} \mathbf{R} \mathbf{J}_0^-, & \mathbf{R}_0^- &= \mathbf{K}_0^- \hat{\mathbf{G}} \mathbf{R} \mathbf{J}_0^+, \\ \mathbf{T}_0^+ &= \mathbf{1} + \mathbf{K}_0^+ \hat{\mathbf{G}} \mathbf{R} \mathbf{J}_0^+, & \mathbf{T}_0^- &= \mathbf{1} + \mathbf{K}_0^- \hat{\mathbf{G}} \mathbf{R} \mathbf{J}_0^-, \\ \mathbf{Q}_0^+ &= \mathbf{K}_0^+ \hat{\mathbf{G}} \hat{\mathbf{T}}, & \mathbf{Q}_0^- &= \mathbf{K}_0^- \hat{\mathbf{G}} \hat{\mathbf{T}}. \end{aligned}$$

Here, the matrices \mathbf{R}_0^\pm and \mathbf{T}_0^\pm are the plane wave reflection and transmission scattering matrices, while the terms

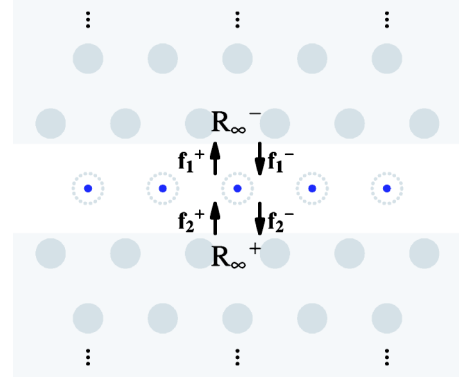


FIG. 3. Modeled structure, consisting of a sourced grating between two semi-infinite stacks, described by reflection matrices \mathbf{R}_∞^\pm . The lower stack has infinite extent in the downward direction and its reflection is described by \mathbf{R}_∞^+ , which relates \mathbf{f}_2^- and \mathbf{f}_2^+ . The appropriate source removes the dotted cylinders along the central row, thus leading to a waveguide.

$\mathbf{Q}_0^\pm \mathbf{Q}$ denote the contributions to the upward and downward going plane wave fields due to the embedded quasiperiodic array of sources \mathbf{Q} . In fact, because the grating has up-down symmetry, it can be shown that

$$\mathbf{R}_0^+ = \mathbf{R}_0^- = \mathbf{R}_0, \quad \mathbf{T}_0^+ = \mathbf{T}_0^- = \mathbf{T}_0. \quad (15)$$

As we shall see in Sec. II D, this symmetry simplifies the formulation and decreases the computation time.

C. Reflection by a stack

We now consider a stack of the gratings discussed in Sec. II B, but without sources. In this way we can create the two-dimensional, semi-infinite array of cylinders shown in the gray regions in the Fig. 3. Between each layer, we represent the field by a plane wave expansion with upward (\mathbf{f}^+) and downward (\mathbf{f}^-) components that we combine into a vector

$$\begin{pmatrix} \mathbf{f}^- \\ \mathbf{f}^+ \end{pmatrix}.$$

Putting $\mathbf{Q} = \mathbf{0}$ in Eq. (14) and rearranging these expressions allows us to relate the fields on either side of the layer in terms of a *transfer matrix* \mathcal{T} [14]. The eigenvalue problem for this matrix is equivalent to finding the Bloch modes of the bulk structure; specifically, if

$$\mathcal{T} \begin{pmatrix} \mathbf{f}^- \\ \mathbf{f}^+ \end{pmatrix} = \mu \begin{pmatrix} \mathbf{f}^- \\ \mathbf{f}^+ \end{pmatrix},$$

then the coefficients \mathbf{f}^\pm determine a Bloch mode with Bloch vector \mathbf{k}_0 , whose scalar products with the lattice vectors $\{\mathbf{e}_1, \mathbf{e}_2\}$ are given by

$$e^{i\mathbf{k}_0 \cdot \mathbf{e}_1} = e^{i\alpha_0 d}, \quad e^{i\mathbf{k}_0 \cdot \mathbf{e}_2} = \mu.$$

The downward propagating Bloch modes are combined to form the columns of the partitioned matrix

$$\begin{pmatrix} \mathbf{F}^- \\ \mathbf{F}^+ \end{pmatrix}.$$

We are interested in determining the reflection properties of a semi-infinite PC, to model the structure in Fig. 3. We see such a crystal extending infinitely in the $-\hat{y}$ direction in gray in the lower half of this figure. Just above this stack, the upward propagating wave \mathbf{f}_2^+ is a reflection of the downward propagating wave \mathbf{f}_2^- . The reflection condition is that there are no Bloch modes propagating upward from $-\infty\hat{y}$. The field should then be composed only of downward propagating Bloch modes. That is,

$$\begin{pmatrix} \mathbf{f}_2^- \\ \mathbf{f}_2^+ \end{pmatrix} = \begin{pmatrix} \mathbf{F}^- \\ \mathbf{F}^+ \end{pmatrix} \mathbf{c}_-,$$

where \mathbf{c}_- are the amplitudes of these Bloch modes. Eliminating \mathbf{c}_- , we deduce

$$\mathbf{f}_2^+ = \mathbf{R}_\infty^+ \mathbf{f}_2^-,$$

where $\mathbf{R}_\infty^+ = \mathbf{F}^+(\mathbf{F}^-)^{-1}$. We can similarly find the reflection matrix \mathbf{R}_∞^- for the stack extending upward; indeed it can be shown that, by up-down symmetry,

$$\mathbf{R}_\infty^+ \stackrel{\text{def}}{=} \mathbf{R}_\infty^- = \mathbf{R}_\infty. \quad (16)$$

A detailed description of this procedure was given earlier [14], and we do not discuss it further here.

D. Formulation for defect modes

1. Solution of the inhomogeneous problem

We now determine the outgoing field (\mathbf{B}) in terms of the fictitious sources (\mathbf{Q}) in Fig. 3. In Sec. II B, we derived Eq. (14) to describe the scattering properties of the grating with embedded sources in terms of the plane wave fields above and below the grating, while in Sec. II C we deduced the reflection conditions imposed by the semi-infinite stacks on these coefficients, i.e.,

$$\mathbf{f}_2^+ = \mathbf{R}_\infty^+ \mathbf{f}_2^-, \quad \mathbf{f}_1^- = \mathbf{R}_\infty^- \mathbf{f}_1^+.$$

By combining these results we derive

$$\begin{aligned} \mathbf{f}_1^- &= \mathbf{R}_\infty^-(\mathbf{R}_0^+ \mathbf{f}_1^+ + \mathbf{T}_0^+ \mathbf{f}_2^+ + \mathbf{Q}_0^+ \mathbf{Q}), \\ \mathbf{f}_2^+ &= \mathbf{R}_\infty^+(\mathbf{R}_0^- \mathbf{f}_2^- + \mathbf{T}_0^- \mathbf{f}_1^- + \mathbf{Q}_0^- \mathbf{Q}). \end{aligned} \quad (17)$$

Although Eqs. (17) can be solved simultaneously, in general, it is convenient to exploit the up-down symmetry, thereby realizing a substantial increase in the computational efficiency of the method. We define

$$\begin{aligned} \mathbf{f}^s &= \frac{1}{2}(\mathbf{f}_1^- + \mathbf{f}_2^+), & \mathbf{f}^a &= \frac{1}{2}(\mathbf{f}_1^- - \mathbf{f}_2^+), \\ \mathbf{Q}_0^s &= \frac{1}{2}(\mathbf{Q}_0^+ + \mathbf{Q}_0^-), & \mathbf{Q}_0^a &= \frac{1}{2}(\mathbf{Q}_0^+ - \mathbf{Q}_0^-), \\ \mathbf{J}_0^s &= \mathbf{J}_0^- + \mathbf{J}_0^+, & \mathbf{J}_0^a &= \mathbf{J}_0^- - \mathbf{J}_0^+. \end{aligned}$$

Employing the results of up-down symmetry mentioned in the previous two subsections, Eq. (17) is replaced by the symmetrized and antisymmetrized forms

$$\mathbf{f}^s = \mathbf{R}_\infty^s [(\mathbf{R}_0 + \mathbf{T}_0) \mathbf{f}^s + \mathbf{Q}_0^s \mathbf{Q}],$$

$$\mathbf{f}^a = \mathbf{R}_\infty^a [(\mathbf{R}_0 - \mathbf{T}_0) \mathbf{f}^a + \mathbf{Q}_0^a \mathbf{Q}],$$

while Eq. (13) becomes

$$\mathbf{B} = \mathbf{G}(\hat{\mathbf{R}}\mathbf{J}_0^s \mathbf{f}^s + \hat{\mathbf{R}}\mathbf{J}_0^a \mathbf{f}^a + \hat{\mathbf{T}}\mathbf{Q}).$$

Hence

$$\mathbf{B} = \mathbf{Z}\mathbf{Q}, \quad (18)$$

where

$$\begin{aligned} \mathbf{Z} = \mathbf{Z}(k, \alpha_0) &= \mathbf{G}\{\hat{\mathbf{R}}\mathbf{J}_0^s[\mathbf{1} - \mathbf{R}_\infty(\mathbf{R}_0 + \mathbf{T}_0)]^{-1}\mathbf{R}_\infty\mathbf{Q}_0^s \\ &\quad + \hat{\mathbf{R}}\mathbf{J}_0^a[\mathbf{1} - \mathbf{R}_\infty(\mathbf{R}_0 - \mathbf{T}_0)]^{-1}\mathbf{R}_\infty\mathbf{Q}_0^a + \hat{\mathbf{T}}\}. \end{aligned}$$

We have thus expressed the outgoing field around the central cylinder in terms of the fictitious source it contains. Note that \mathbf{Z} incorporates the effects of scattering by the infinite number of surrounding cylinders and depends on the transverse wave number k and $\alpha_0 = k_{0x}$, the x component of the Bloch vector. The other component of the Bloch vector is included through \mathbf{R}_∞ .

2. One-dimensional defect (waveguide) modes

Earlier we mentioned that the construction of a defect mode requires the superposition of all quasiperiodic solutions, necessitating an integration over the first Brillouin zone, a result we detail shortly. Before doing so, however, we demonstrate that it is possible to proceed directly from (18) to model a one-dimensional defect mode, i.e., a waveguide mode, without the need for any integration.

To do this, we set $\mathbf{B} = \mathbf{0}$, as in Sec. II A, thereby setting the response (outgoing) field from the central cylinder to zero. Since all cylinders are quasiperiodically phased according to Bloch's theorem, setting $\mathbf{B} = \mathbf{0}$ removes not only the central cylinder but all cylinders of the grating. We thus derive a mode of the waveguide structure (Fig. 3) characterized by a nontrivial solution of

$$\mathbf{Z}\mathbf{Q} = \mathbf{0}. \quad (19)$$

For a fixed frequency (i.e., a given k), we may vary the x component of the Bloch vector, α_0 , so that \mathbf{Z} becomes singular. That is,

$$\det[\mathbf{Z}(k, \alpha_0)] = 0.$$

The source \mathbf{Q} for which the outgoing field \mathbf{B} vanishes around each grating cylinder is found from the null space of $\mathbf{Z}(k, \alpha_0)$, from which the mode can be reconstructed.

Similarly we can model a waveguide obtained by altering the central row of cylinders, e.g., varying their optical constants or their radii. To mimic the altered cylinders, the external fields must satisfy the equivalent of Eq. (2), but without the fictitious source, for the new cylinder radius and index, namely,

$$\mathbf{B} = \hat{\mathbf{R}}_1 \mathbf{A}. \quad (20)$$

Combining Eq. (20) with Eqs. (2) and (18), we obtain

$$[(1 - \hat{\mathbf{R}}_1 \hat{\mathbf{R}}^{-1})\bar{\mathbf{Z}} + \hat{\mathbf{R}}_1 \hat{\mathbf{R}}^{-1} \hat{\mathbf{T}}]\mathbf{Q} = \mathbf{0}.$$

Again, α_0 is varied to make this matrix singular, and the null space produces \mathbf{Q} which defines the mode.

3. Two-dimensional defect modes

To model a mode of a point defect, we must employ the second key idea, namely, its construction from the superposition of the solutions of all quasiperiodic field problems formed by integrating over α_0 within the first Brillouin zone. The superposed solution thus satisfies the Helmholtz equation and the boundary conditions (which depend only on k and not on α_0) and is associated with an averaged fictitious source distribution which, in cylinder j , is $\mathbf{Q} \int_{-\pi/d}^{\pi/d} \exp(i\alpha_0 j d) d\alpha_0$. This is the crucial step in the method, with the Brillouin zone integration maintaining the source in the central cylinder ($\mathbf{j}=0$) which is independent of α_0 , while eliminating all the other sources due to the Bloch factor $e^{i\alpha_0 j d}$.

The superposed solution, corresponding to a single source (Fig. 1) in the central cylinder, thus follows by integrating

$$\mathbf{B}(k, \alpha_0) = \mathbf{Z}(k, \alpha_0) \mathbf{Q}(k) \quad (21)$$

over the first Brillouin zone with the averaging operator

$$\frac{d}{2\pi} \int_{-\pi/d}^{\pi/d} d\alpha_0.$$

We thus derive

$$\bar{\mathbf{B}}(k) = \bar{\mathbf{Z}}(k) \mathbf{Q}(k), \quad (22)$$

where the overbar denotes an averaged quantity.

We may now proceed, as in the waveguide case, to find the modes of a defect structure with the central cylinder removed or altered, by solving

$$\bar{\mathbf{Z}}\mathbf{Q} = \mathbf{0},$$

or

$$[(1 - \hat{\mathbf{R}}_1 \hat{\mathbf{R}}^{-1})\bar{\mathbf{Z}} + \hat{\mathbf{R}}_1 \hat{\mathbf{R}}^{-1} \hat{\mathbf{T}}]\mathbf{Q} = \mathbf{0},$$

respectively. The free space wave number k , or equivalently the normalized frequency

$$f = kd/(2\pi), \quad (23)$$

is varied to make the relevant matrix singular. Again, the null space determines \mathbf{Q} , from which the fields may be reconstructed.

E. Three-dimensional fields

Thus far, we have assumed an in-plane solution for either \mathbf{E}_{\parallel} or \mathbf{H}_{\parallel} polarization, so only one of the fields has a $\hat{\mathbf{z}}$ component, which is constant in z . However, in the three-dimensional case, as occurs when solving propagation problems for PCFs, the fields have an $e^{i\beta z}$ dependence. This causes the $\hat{\mathbf{z}}$ components of the two fields to couple at the cylindrical interfaces and requires that both quantities be in-

cluded in the solution of the field problem. For notational convenience, we combine these into a single vector; for instance we replace \mathbf{A} by

$$\begin{pmatrix} \mathbf{A}^E \\ \mathbf{A}^K \end{pmatrix},$$

partitioned into two blocks containing a vector of electric field coefficients \mathbf{A}^E and a vector of magnetic field coefficients \mathbf{A}^K . Here we have introduced $\mathbf{K} = Z_0 \mathbf{H}$, where Z_0 is the vacuum impedance, so \mathbf{E} and \mathbf{K} have the same units. Similarly, all of the above matrices double in dimension; for instance, in block matrix notation, the Toeplitz matrix of lattice sums, \mathbf{S} , is replaced by

$$\begin{pmatrix} \mathbf{S} & \mathbf{0} \\ \mathbf{0} & \mathbf{S} \end{pmatrix}.$$

Rather than being diagonal, the boundary condition matrices of (2) are now composed of diagonal blocks; for instance $\hat{\mathbf{R}}$ is replaced by

$$\begin{pmatrix} \hat{\mathbf{R}}^{EE} & \hat{\mathbf{R}}^{EK} \\ \hat{\mathbf{R}}^{KE} & \hat{\mathbf{R}}^{KK} \end{pmatrix},$$

where each submatrix is diagonal, in the case of circular cylinders. Their exact forms are given in Refs. [10,18]. It should also be noted that the magnitude of the in-plane component of the wave vector is now given by

$$k^{\pm} = \sqrt{n^{\pm 2} k^2 - \beta^2}.$$

In general, the matrices $\hat{\mathbf{R}}^{EK}$ and $\hat{\mathbf{R}}^{KE}$ do not vanish and thus the electric and magnetic fields problems are coupled. In the case of in-plane incidence, however, both $\hat{\mathbf{R}}^{EK}$ and $\hat{\mathbf{R}}^{KE}$ vanish, and thus all matrices in the formulation are of block diagonal form, leading to decoupled \mathbf{E}_{\parallel} and \mathbf{H}_{\parallel} polarized solutions.

From this point on, the formulation is almost identical to that of Sec. II B onward, the only exception being the relations resulting from up-down symmetry; because the magnetic field is a pseudovector, it is reversed when we reflect in the xz plane. Thus Eqs. (15) and (16) become

$$\mathbf{R}_0^- = \mathbf{Y} \mathbf{R}_0^+ \mathbf{Y}, \quad \mathbf{T}_0^- = \mathbf{Y} \mathbf{T}_0^+ \mathbf{Y}, \quad \mathbf{R}_{\infty}^- = \mathbf{Y} \mathbf{R}_{\infty}^+ \mathbf{Y},$$

where

$$\mathbf{Y} = \begin{pmatrix} \mathbf{1} & \mathbf{0} \\ \mathbf{0} & -\mathbf{1} \end{pmatrix},$$

written as a block matrix partitioned into electric and magnetic plane wave coefficients.

The search routine for defect modes in three-dimensional problems is slightly different, being tailored to the practice usually adopted for PCFs. Whereas, in the two-dimensional case we varied the free space wave number k , for a PCF we fix k and vary the propagation constant β , or equivalently the effective index

$$n_{\text{eff}} = \beta/k,$$

to make the relevant matrix singular.

III. IMPLEMENTATION

The theory of Sec. II was implemented numerically to model defects in PCs and PCFs. First this requires the infinite dimensional matrices to be truncated; that is, the cylindrical harmonic index l and plane wave order index p , which range from $-\infty$ to ∞ , are restricted to

$$-N_J \leq l \leq N_J, \quad -N_p \leq p \leq N_p. \quad (24)$$

Central to the method presented in Sec. II B was the calculation of the matrix

$$\mathbf{G} = (\mathbf{1} - \hat{\mathbf{R}}\mathbf{S})^{-1}. \quad (25)$$

However, the matrix $\mathbf{1} - \hat{\mathbf{R}}\mathbf{S}$ is poorly conditioned for numerical inversion. By studying the asymptotic behavior of the elements of $\hat{\mathbf{R}}$ and \mathbf{S} , it can be seen that for the purposes of calculation, Eq. (25) should be replaced by

$$\mathbf{G} = \mathcal{C}[\mathcal{C}^{-1}(\mathbf{1} - \hat{\mathbf{R}}\mathbf{S})\mathcal{C}]^{-1}\mathcal{C}^{-1},$$

where \mathcal{C} is the diagonal matrix defined by

$$C_{ll} = \left(\frac{k^+ a}{2}\right)^{|l|} \frac{1}{|l|!}.$$

This allows us to calculate $\mathbf{Z}(k, \alpha_0)$ numerically.

To obtain $\bar{\mathbf{Z}}$, we approximate the Brillouin averaging by a numerical integration

$$\bar{\mathbf{Z}}(k) \approx \sum_{l=0}^N w_l \mathbf{Z}\left(k, \frac{2\pi}{d} x_l\right),$$

where (w_l, x_l) are chosen according to some integration rule. We generally use Gaussian quadratures, which are well suited to the behavior of the integrand. However, assume momentarily that the trapezoidal rule with N points is used to replace the integral; then we leave, in effect, sources in every N th cylinder. Therefore, although the theory we have presented deals with a truly infinite structure, the structure we then ultimately model has every N th cylinder along the central row missing or altered. Nevertheless, unlike a supercell calculation, the method can calculate defect modes with extremely large spatial extent, as we discuss in Sec. VI.

Our theory has been implemented in MATHEMATICA [19], with the lattice sums calculated in a FORTRAN routine linked to the MATHEMATICA routines using the MATHLINK toolkit [19]. This implementation is thus a successful prototype, but not one that has been optimized for efficiency. All calculations reported here were undertaken using a 2.4 GHz Pentium 4 workstation running under Microsoft Windows XP, with timings referring to this system.

IV. VERIFICATION

A. Waveguide mode

In Sec. II D 2 we investigated a waveguide mode in order to verify numerically the fictitious sources concept on which the method relies. Consider a square lattice structure, consisting of dielectric cylinders of index $n=3$ and radius a

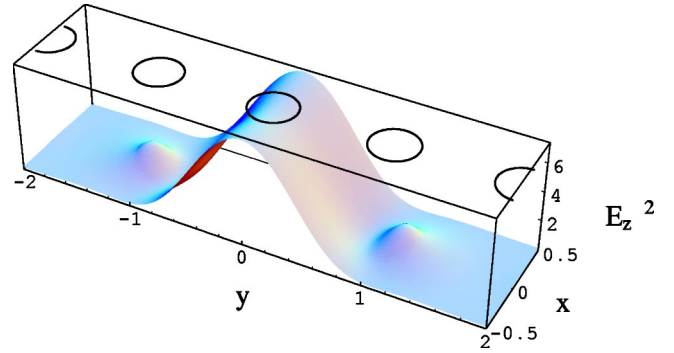


FIG. 4. Squared modulus of the electric field in an \mathbf{E}_{\parallel} polarized waveguide mode calculated with the FSS method, plotted over one period in the x direction. Circles at the top indicate the cylinders. The corresponding result obtained by RSoft BandSOLVE differs by a maximum of 1 part in 10^3 .

$=0.2d$, surrounded by air. One row of cylinders is removed to form a waveguide. At a normalized frequency of $f=0.4$ [see Eq. (23)], the FSS method found an \mathbf{E}_{\parallel} polarized mode with Bloch component $\alpha_0=1.82528$ (Fig. 4). The value of α_0 obtained by another code, developed by Botten *et al.* [13,20], that combines a multipole calculation with a Bloch mode analysis, agreed to the six figures shown. This value of α_0 was used as the input for a supercell calculation, using the RSoft module BandSOLVE [21], which returned a normalized frequency of 0.40006. The relative discrepancy of $<0.02\%$ is mainly due to the number of plane waves used in the supercell calculation, namely 32×256 ; increasing this to 64×512 reduced the discrepancy to $<0.005\%$. In contrast, our calculation obtained results accurate to 11 significant figures using multipole series truncation of $N_J=6$ and plane wave series truncation of $N_p=3$.

B. PCF modes

The FSS method has been used to find modes in PCFs, using the parameters $N_J=9$, $N_p=4$, and $N=80$. The wavelength was chosen small enough that the modes were well confined. This allowed them to be compared to those of a finite structure, calculated using other multipole software developed by Kuhlmeier [22,23]. The latter was also used to plot the modes.

In all cases the PCF structure consisted of air holes in silica, the latter having a refractive index of 1.45. Figure 5 shows the fundamental modes of an infinite structure and a finite structure with seven rings, both with hole radius $a=0.12d$ and at wavelength $\lambda=0.133d$. The effective indices were found to be 1.4492264513 for the infinite structure and 1.4492264520 + $1 \times 10^{-12}i$ for the finite structure. The loss of the finite structure mode, which is proportional to $\text{Im}(n_{\text{eff}})$, is very low. This indicates that the mode is well confined, explaining the good agreement between the effective indices found.

Figure 6 shows the same comparison for the second mode, but with hole radius $a=0.25d$ and at a wavelength $\lambda=0.3d$. The effective indices were now 1.436222 for the infinite structure and 1.436225 + $6 \times 10^{-8}i$ for the finite struc-

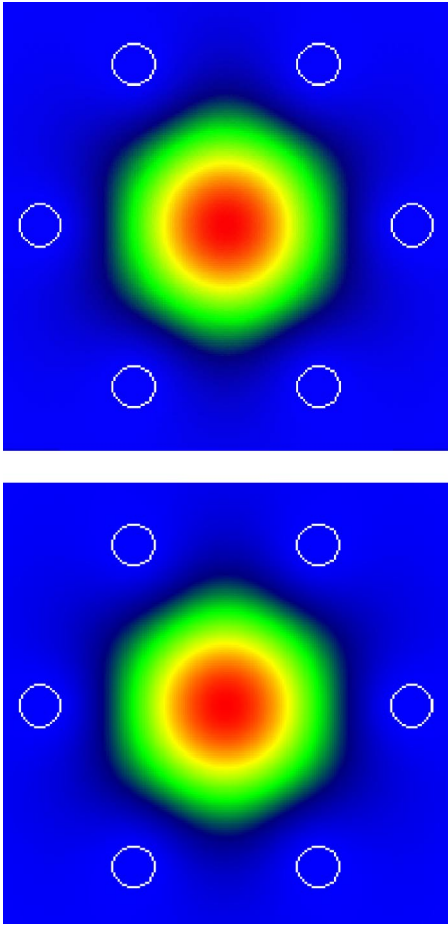


FIG. 5. The \hat{z} component of the Poynting vector $\mathcal{S} \propto \mathbf{E} \times \mathbf{H}$ of the fundamental mode in an infinite structure (top) and a finite structure with seven rings (bottom) for $a=0.12d$, $\lambda=0.133d$, and $n=1.5$.

ture. The imaginary part of the latter is larger than for the fundamental mode, and the difference in the real parts of the effective indices between is correspondingly greater.

To ensure that the parameters chosen above are sufficient, we varied them and observe the stability of n_{eff} (Table I). All but the final calculation used the trapezoidal rule for the numerical integration; the last employed Gaussian quadratures. As we discuss further in Sec. VI, the stability of the root confirms that the method is accurately modeling an infinite structure.

Due to the high symmetry of the geometry, the fundamental PCF mode studied is doubly degenerate. Our numerical results are consistent with this: the effective indices obtained for the modes differ only slightly (by roughly 3×10^{-12}), which is smaller than the accuracy of the calculation.

V. SPATIALLY EXTENDED MODES

The results in Sec. IV B, while validating the FSS method, do not demonstrate the unique advantage that it affords, namely, in handling the difficult cases in which methods which assume a finite structure, either explicitly or implicitly, fail. Accordingly, we show the strength of the

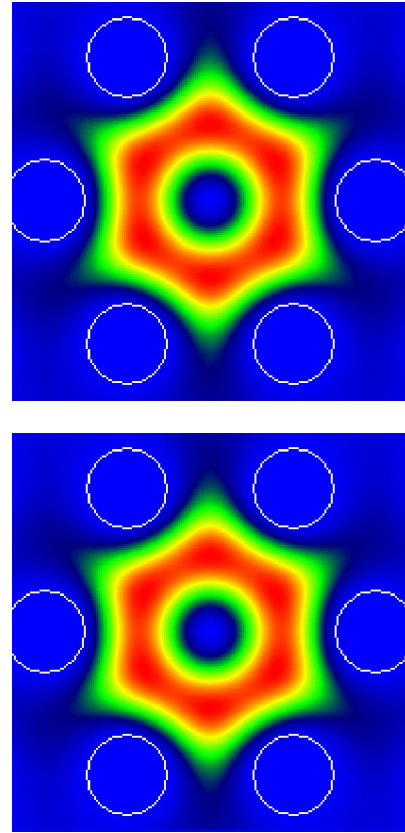


FIG. 6. As in Fig. 5 but for the second mode and $a=0.25d$, $\lambda=0.3d$, and $n=1.5$.

technique by calculating a poorly confined defect mode near the edge of the band gap. Because of the large spatial extent of the mode, such a calculation using existing methods cannot achieve the same accuracy.

We consider the same square lattice as that from which the waveguide structure was obtained. The central cylinder radius is reduced to $0.17d$. With the parameters $N_J=6$, $N_p=3$, and a Gaussian integration with $N=40$ points, the FSS method took less than 3 min to find a defect mode at normalized frequency 0.321 035 154 65 (Fig. 7). A convergence study demonstrated that the result is accurate to the 11 figures shown.

TABLE I. Effective index n_{eff} for the structure in Fig. 5 as a function of the numerical parameters N_J and N_p [Eq. (24)], and the number of integration points N .

N_J	N_p	N	n_{eff}
9	4	80	1.449226451342261
6	4	80	1.4492264513
3	4	80	1.449226452014651
9	3	80	1.449226451340456
9	2	80	1.449226451345897
9	4	40	1.449226451343528
9	4	120	1.449226451340771
9	4	80	1.449226451340257

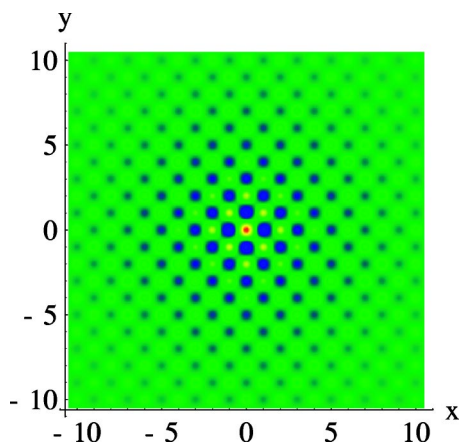


FIG. 7. Electric field in an E_{\parallel} polarized defect mode for a single cylinder defect in a square symmetric lattice with $a=0.2d$ and $n=3$. Cylinders are placed on the grid of points with integer coefficients.

The mode can also be found using an RSoft BandSOLVE [21] calculation in comparable time. However, the same accuracy cannot be achieved; Fig. 8 shows the difference between the frequency of the supercell calculation and the frequency of the mode, as a function of supercell size. The three curves correspond to 8, 12, and 24 plane waves per unit cell of the original lattice. It is clear that a very large supercell is required because of the spatial extent of the mode.

Because the bulk of the computation time for the FSS method involves calculating $\bar{\mathbf{Z}}$, the hole radius can easily be varied at fixed frequency. For example, Fig. 9 shows the frequency of the above defect mode versus hole radius. Using $N_J=6$, $N_p=3$, and $N=80$, the 60 data points for the figure took less than 7 min to produce.

VI. CONCLUSIONS

To date, all methods for computing defect modes have been approximations, relying either on perturbation tech-

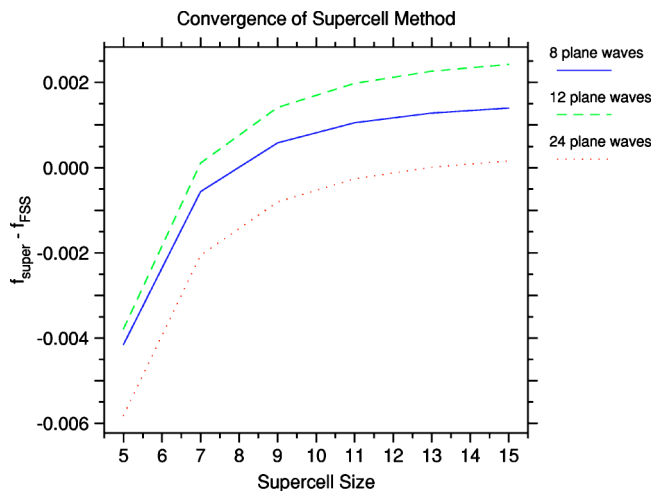


FIG. 8. Frequency error versus supercell size, for different numbers of plane waves per unit cell, when calculating the mode in Fig. 7 using a supercell.

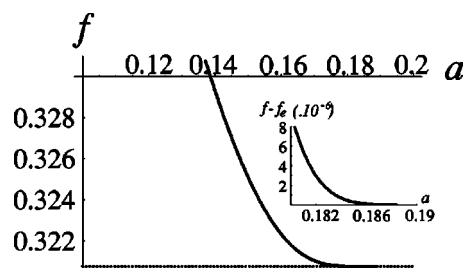


FIG. 9. Normalized frequency f of the defect mode if one cylinder in the regular square lattice is reduced to radius a . The dotted line indicates the lower edge of the band gap f_e . Inset shows a closeup, indicating $f-f_e$ versus a .

niques or embedding in the model an explicit or implicit assumption of a finite structure. The method that we have outlined here is different in that it can model exactly defect modes in structures which have a truly infinite cladding. It thus can handle those extreme situations in which the mode becomes arbitrarily extended, such as near cutoff, for which alternative methods either fail completely or become either inefficient or inaccurate.

While the theory is exact, in the sense that it models geometrically infinite structures, any numerical implementation introduces some truncation errors. The most significant potential source of error lies in the numerical evaluation of the Brillouin zone integration. Recall from Sec. III that if the integral is approximated by the trapezoidal rule, then we essentially model a structure with missing or altered cylinders placed periodically along the central row. Thus, although the method theoretically models an infinite structure, our numerical implementation is apparently very similar to a supercell technique. Nevertheless, our modeled structure is truly infinite in the $\pm\hat{y}$ directions, and thus the computation time increases only linearly with the artificial period N in the \hat{x} direction. In contrast, the computation time for supercell methods must increase at least quadratically, since the matrices scale in size quadratically with N . Recall also that the convergence study of Sec. IV B found the root to be very stable when varying not only the number of integration points, but also the integration rule; Gaussian quadrature has irregularly spaced points, and so does not model an equivalent supercell structure. Even at $\lambda=1.6d$, the highest wavelength studied, a Gaussian rule with 80 points was sufficient to find the effective index of the fundamental PCF mode to seven figures of accuracy. We thus conclude that we are modeling a truly infinite structure.

With the method's unique capabilities for handling spatially extended modes demonstrated, we plan to apply the tool to study applications not accessible by other means. In particular, we intend to use it to study the endlessly single mode property of PCFs and to clarify the issue concerning the existence, or otherwise, of a cutoff of the fundamental mode. We also plan to extend the method to remove the current restriction of a single defect, allowing us to study more general defect geometries.

ACKNOWLEDGMENT

This work was produced with the assistance of the Australian Research Council under the ARC Centres of Excellence program.

- [1] J. D. Joannopoulos, R. D. Meade, and J. N. Winn, *Photonic Crystals: Molding the Flow of Light* (Princeton University Press, Princeton, NJ, 1995).
- [2] A. Bjarklev, J. Broeng, and A. S. Bjarklev, *Photonic Crystal Fibres* (Kluwer Academic Publishers, Norwell, MA, 2003).
- [3] M. Notomi, A. Shinya, E. Kuramochi, I. Yokohama, C. Takahashi, K. Yamada, J.-I. Takahashi, T. Kawashima, and S. Kawakami, *IEICE Trans.* **85C**, 1025 (2002).
- [4] O. Painter, R. K. Lee, A. Scherer, A. Yariv, J. D. O'Brien, P. D. Dapkus, and I. Kim, *Science* **284**, 1819 (1999).
- [5] Y. Akahane, T. Asano, B. S. Song, and S. Noda, *Nature (London)* **425**, 944 (2003).
- [6] J. C. Knight, J. Broeng, T. A. Birks, and P. S. J. Russell, *Science* **282**, 1476 (1998).
- [7] K. M. Ho, C. T. Chan, and C. M. Soukoulis, *Phys. Rev. Lett.* **65**, 3152 (1990).
- [8] S. G. Johnson and J. D. Joannopoulos, *Opt. Express* **8**, 173 (2001).
- [9] T. M. Monro, D. J. Richardson, N. G. R. Broderick, and P. J. Bennett, *J. Lightwave Technol.* **17**, 1093 (1999).
- [10] T. P. White, B. T. Kuhlmeier, R. C. McPhedran, D. Maystre, G. Renversez, C. Martijn de Sterke, and L. C. Botten, *J. Opt. Soc. Am. B* **19**, 2322 (2002).
- [11] L. Poladian, N. A. Issa, and T. M. Monro, *Opt. Express* **10**, 449 (2002).
- [12] F. Brechet, J. Marcou, D. Pagnoux, and P. Roy, *Opt. Fiber Technol.* **6**, 181 (2000).
- [13] T. N. Langtry, L. C. Botten, C. Martijn de Sterke, A. A. Asatryan, and R. C. McPhedran, *Phys. Rev. E* **68**, 026611 (2003).
- [14] L. C. Botten, N. A. Nicorovici, R. C. McPhedran, C. Martijn de Sterke, and A. A. Asatryan, *Phys. Rev. E* **64** 046603 (2001).
- [15] C. G. Poulton, R. C. McPhedran, N. A. Nicorovici, and L. C. Botten, in *IUTAM Symposium on Asymptotics, Singularities and Homogenisation in Problems of Mechanics*, edited by A. B. Movchan (Kluwer Academic Publishers, Dordrecht, 2003), pp. 181–190.
- [16] L. C. Botten, N. A. Nicorovici, A. A. Asatryan, R. C. McPhedran, C. Martijn de Sterke, and P. A. Robinson, *J. Opt. Soc. Am. A* **17**, 2165 (2000).
- [17] L. C. Botten, N. A. Nicorovici, A. A. Asatryan, R. C. McPhedran, C. Martijn de Sterke, and P. A. Robinson, *J. Opt. Soc. Am. A* **17**, 2177 (2000).
- [18] T. P. White, B. T. Kuhlmeier, R. C. McPhedran, D. Maystre, G. Renversez, C. Martijn de Sterke, and L. C. Botten, *J. Opt. Soc. Am. B* **20**, 1581 (2003).
- [19] Wolfram Research, computer code MATHEMATICA, Ver. 5.0, 2003.
- [20] L. C. Botten, T. P. White, C. Martijn de Sterke, R. C. McPhedran, A. A. Asatryan, and T. N. Langtry, *Opt. Express* **12**, 1592 (2004).
- [21] RSoft Design Group, computer code BandSOLVE, available at http://www.rsftdesign.com/products/component_design/BandSOLVE/
- [22] T. P. White, B. T. Kuhlmeier, R. C. McPhedran, D. Maystre, G. Renversez, C. Martijn de Sterke, and L. C. Botten, *J. Opt. Soc. Am. B* **19**, 2331 (2002).
- [23] B. T. Kuhlmeier, computer code CUDOS MOF Utilities, available at <http://www.physics.usyd.edu.au/cudos/mofsoftware/index.html>